Catalysis Today 155 (2010) 75–83

Contents lists available at ScienceDirect

Catalysis Today

journal homepage: www.elsevier.com/locate/cattod

Catalytic partial oxidation of n-butane over Rh catalysts for solid oxide fuel cell applications

Seyed-A. Seyed-Reihani [1], Gregory S. Jackson *

Department of Mechanical Engineering, 2181 Glen Martin Hall, University of Maryland, College Park, MD 20742, USA

ARTICLE INFO

Article history:
Available online 23 May 2009

Keywords:
Partial oxidation
Butane
Rhodium
Catalysis
Solid oxide fuel cells

ABSTRACT

Catalytic partial oxidation (CPOx) of n-butane in O_2/Ar mixtures at ratios of 1/3.76 has been investigated over Rh catalysis impregnated in γ-Al_2O_3 washcoat supports coated on α-Al_2O_3 ceramic foam monoliths. The impact of heat loss on Rh-based CPOx reactor performance for small-scale SOFC application is tested here by varying reactor lengths, insulation, and flow conditions. Results for a C/O ratio = 1.0 and T_{in} = 300 °C indicate the n-butane conversion and H_2 and CO selectivity depend strongly upon reactor temperature and thus heat lost through the external reactor walls. Because heat loss does not scale with flow rate, higher flow rates for catalyst contact times approaching 15 ms increase fuel conversion and syngas selectivity. Furthermore, shortening catalyst length (from 10 to 5 mm) also reduces heat loss and increases fuel conversion and H_2 selectivity. CO selectivity, however, drops with the shorter length. These results suggest that for the conditions tested, butane conversion and H_2 production occur rapidly within the first couple of mm in the reactor, whereas CO production occurs more broadly throughout the reactor length. This study provides valuable insight into the conditions needed for good CPOx performance for fuel processing in small-scale SOFC applications.

1. Introduction

Development of solid oxide fuel cell (SOFC) systems running on hydrocarbons including liquid fuels and light hydrocarbons such as n-butane is beginning to show the attractiveness of SOFCs for small-scale power applications of <5 kW. Although it has been shown that direct utilization of hydrocarbons in SOFCs is a possibility with internal reforming for certain operating conditions, SOFC anode materials and architectures [1,2], stable SOFC operation at higher power densities can be achieved with external reforming [3,4]. For small power SOFC applications, fuel reforming and adequate preheating of inlet flows must be done in a volumetrically efficient manner. As such, catalytic partial oxidation (CPOx) of hydrocarbon fuels has been considered attractive because the rapid kinetics permit volumetrically efficient syngas production without excessive amounts of fuel preheating [5–9]. In comparison to endothermic steam reforming of hydrocarbons, CPOx provides superior start-up and transient response and reduces the heat input to the fuel stream – both of which are critical in small-scale power applications. Improving fundamental understanding of CPOx reactors with higher hydrocarbons can provide a basis for designing/optimizing systems for size and operability in various small-scale SOFC systems.

To understand the unique demands of small-scale SOFCs on CPOx reactors, Fig. 1 provides a schematic of an idealized SOFC system with a tightly integrated CPOx fuel processor, which provides both a H_2/CO-rich mixture for the anode flow and general heating for both incoming flows. In such a configuration, waste heat recovery from the anode exhaust combustor can provide preheated air temperatures of 300 °C or higher for the CPOx reactor depending on heat losses along the outer wall of the air passages. In addition, internal heat exchange will occur from the CPOx to the surrounding air flow as indicated in the expanded view of the CPOx reactor in Fig. 1. It is important to understand how non-adiabatic operating conditions of the CPOx reactor will influence fuel conversion and product selectivity.

Early studies by Schmidt and co-workers on CPOx of higher hydrocarbons focused primarily on supported Rh and Pt catalysts in short τ_{res} reactors under near adiabatic conditions [10–12]. Their work indicated Rh catalysts have superior selectivity to syngas, and as such, supported Rh is the focus of this study. These and other studies on CPOx of higher hydrocarbons on Rh catalysts [5,13,14] still leave uncertainties as to the coupling of thermal energy transport and reactor performance in terms of fuel conversion and H_2 and CO selectivities. This is particularly important because the

* Corresponding author. Tel.: +1 301 405 2368; fax: +1 301 405 2025.
E-mail address: gsjackso@umd.edu (G.S. Jackson).
[1] Present address: Massachusetts Institute of Technology, Department of Chemical Engineering, 66-225 and 31-168A, 77 Massachusetts Avenue, Cambridge, MA 02139-4307, USA.

0920-5861/$ – see front matter © 2009 Elsevier B.V. All rights reserved.
doi:10.1016/j.cattod.2009.03.032

Nomenclature

$Conv_k$	conversion of species k in the reactor
$\bar{h}_{k,in}$	enthalpy of species k at inlet flow temperature
$\bar{h}_{k,out}$	enthalpy of species k at downstream (exit) temperature of the catalytic foam monolith
$\dot{n}_{in}$	molar flow rate at downstream face of catalytic foam monolith
$\dot{n}_{out}$	molar flow rate at downstream face of catalytic foam monolith
$\dot{q}_{loss}$	calculated heat loss per unit flow of mass through the reactor
$S_{k,m}$	selectivity of species k with respect to atom m
T_{down}	measured temperature of downstream face of catalytic foam monolith
T_{in}	inlet flow temperature and also controlled furnace temperature
T_{up}	measured temperature of upstream face of catalytic foam monolith
$\dot{V}_{tot,in}$	standard volumetric flow rate supplied to the reactor
$\bar{W}_{in}$	mean molecular weight of inlet flow
$\bar{W}_{out}$	mean molecular weight of exhaust flow
$X_{k,in}$	inlet mole fraction of species k
$X_{k,out}$	measured outlet mole fraction of species k
$\nu_{k,m}$	number of m atoms in molecule of species k
ϕ	equivalence ratio of fuel and air mixture into catalyst
τ_{res}	catalyst contact time

rapid heat release in the first few mm of a CPOx reactor can be driven by direct partial oxidation to H_2/CO and/or complete oxidation to H_2O/CO_2 [6,15] and downstream reactor cooling may significantly impact product selectivity and thus SOFC performance.

A recent study by the authors [16] explored how operating conditions (C/O ratios, T_{in}, and flow rate) and reactor adiabadicity influence CPOx reactor performance for a fixed reactor. The results indicated how relatively small increases in reactor heat loss can significantly reduce both fuel conversion and H_2 selectivity. The study also indicated that for effective residence times $\tau_{res} > 20$ ms, increased reactor flow rates can improve fuel conversion and H_2 selectivity because of increased heat release rates and subsequently higher reactor temperatures. The present study builds on that work by exploring how reactor length can impact the effect of operating conditions and heat loss on CPOx of n-C_4H_{10}. The CPOx reactors with supported Rh catalysts on γ-Al_2O_3 foams are examined both during transient start-up and steady-state conditions that may be expected in small-scale SOFC applications and will thus provide a basis for improved CPOx reactor design for such systems.

2. Experimental

2.1. Catalytic reactor preparation

The CPOx reactors in this study consist of extruded porous α-Al_2O_3 ceramic foams (15 mm in diameter, 5 or 10 mm in length), which are coated with γ-Al_2O_3-washcoat-supported Rh catalysts with pore densities of 80 ppi (pores per linear inch). Details of the coating process and the reactor set-up are provided in [16] and are only summarized here. A γ-Al_2O_3-slurry solution is applied and baked at 400 °C for 6 h to form a thin porous washcoat (20–30 μm thick) on the ceramic foam substrate. The washcoat is impregnated with an aqueous solution of $Rh(NO_3)_3{\cdot}2H_2O$ via an initial wetting and then dipping of the foam monolith in a sonicated solution for 1 h. The impregnated washcoat is dried at 150 °C for 1/2 h and then at room temperature overnight before calcination in air at 600 °C for 4 h. This catalyst coating process was repeated such that the final loading of Rh based on weight (after reduction in H_2) was 2.0% of the total coating. Scanning electron micrograph images of the coated foams after being tested for 10 h are shown in Fig. 2a and b. The lower resolution image in Fig. 2a provides a perspective of the

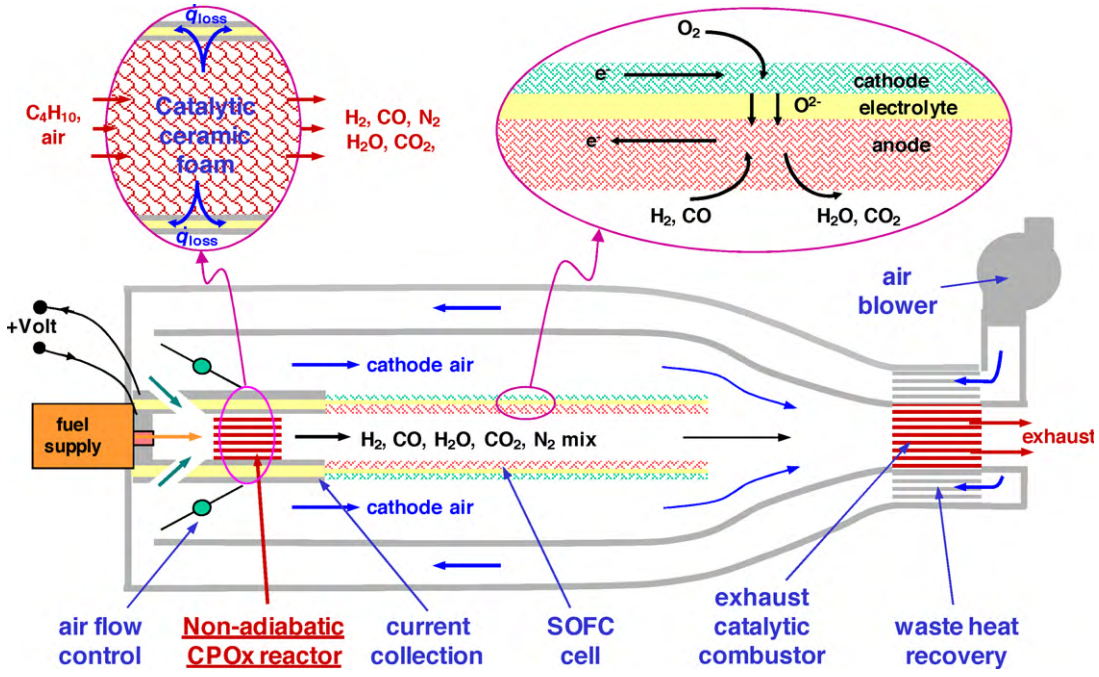

Fig. 1. Schematic (not to scale) showing idealized SOFC system with integrated catalytic partial oxidation reactor (operating in a non-adiabatic mode), a tubular SOFC membrane electrode assembly, and a waste fuel combustor/recuperator for air preheating.

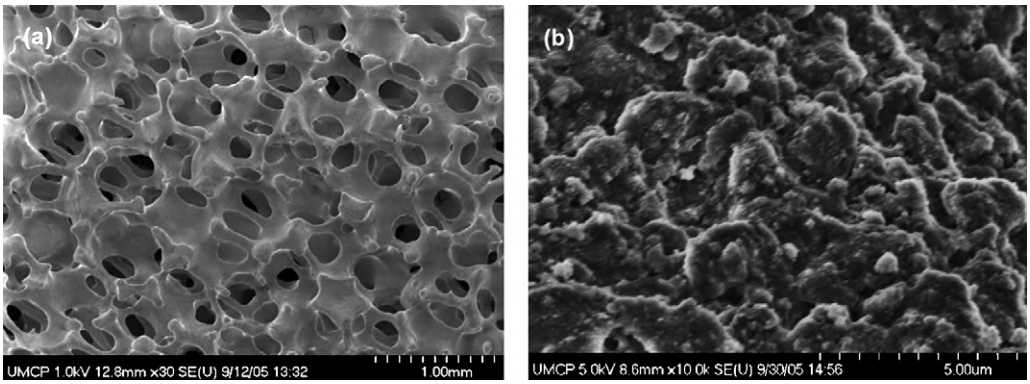

Fig. 2. (a) Scanning electron micrograph of typical pores in an 80 ppi α-Al_2O_3 foam after coating with γ-Al_2O_3 washcoat and impregnation with Rh-catalyst and (b) higher magnification micrograph showing micro-structure of γ-Al_2O_3 washcoat and distribution of Rh catalyst particles.

high foam porosity $\varepsilon \approx 83\%$, and the higher resolution image in Fig. 2b shows washcoat structure and Rh particles with sizes below 200 nm.

The CPOx reactor performed steadily over periods of 10 h or more. In agreement with other studies testing under similar conditions [14], some carbon deposition is observed after reactor testing, but no deactivation associated with carbon deposition is indicated. The carbon deposition may occur during reactor shut-down because O_2 is reduced first to avoid stoichiometric fuel–O_2 ratios. Because of this carbon deposition, fresh catalytic foams were prepared for each set of tests to minimize the possibility of reactor degradation [14].

2.2. Experimental apparatus and method

The Rh/γ-Al_2O_3 coated foam monolith is placed inside a 17 mm diameter quartz tube between two uncoated ceramic foams with a reduced pore density of 45 ppi. The uncoated foams reduce heat loss from radiation in the axial direction. The set of ceramic foams are wrapped with thin Fiberfrax™ silica–alumina cloth to prevent gas bypass between the catalyst and the inner quartz tube wall. The entire assembly is placed in a tubular furnace which is set at the desired test inlet temperature T_{in}. Quartz wool and a quartz frit are placed in the tube upstream of the ceramic foams in order to ensure that the reactant flows reach the desired T_{in} set by the furnace controller. To increase the adiabadicity of the reactor, some tests are conducted with Al_2O_3 fiber blanket around the quartz tube in order to reduce heat loss from the side walls of the reactor.

Temperatures at the upstream and downstream face of the catalytic foam (T_{up} and T_{down} respectively) are measured by two K-type thermocouples inserted through centrally bored holes in the uncoated foam monoliths. The measurements for T_{up} can show significant variation because of the very strong gradient between the catalytic washcoat and the surrounding gas flow in the front region of the reactor [17,18]. Thus, while T_{up} measurements are provided, trends cannot be reliably used to resolve critical aspects of the reaction mechanism. The lack of significant exothermic catalytic reactions at the downstream face implies that gas and surface temperatures are nearly equilibrated as shown in models of CH_4 CPOx reactors [19]. This allows for T_{down} measurements to give an accurate assessment of the downstream gas temperature. Thus, T_{down} is used to assess reactor performance as presented below.

Ultra-pure grade O_2 and Ar (>99.9%) are mixed in a ratio of 1 to 3.76, and n-C_4H_{10} is injected into the O_2/Ar mixture at room temperature before the flows enter the reactor quartz tube. The individual gas flows are controlled by electronic mass flow controllers with an accuracy of ±1% full scale.

The CPOx effluent is sampled at the downstream face of the coated foam monolith and transported out of the furnace via a heated capillary (~100 °C) tube to a magnetic sector mass spectrometer (ThermoFisher VG Prima δB). Ar instead of N_2 is used as the diluent because the main N_2 peak overlaps with the main CO peak at 28 amu. Mass spectrometer signals are translated into species mole fractions using a MATLAB-based analysis tool based on calibrated peak sensitivities. Spectrograms are collected every 15 s to provide transient evolution of outlet species concentrations. The calculated balances of C and O atoms from the exhaust analysis are within ±9% for all conditions except at the lowest C_4H_{10} conversion condition (non-insulated reactor with L_{reac} = 10 mm at lowest flow rate) where the C balance is at 13%. H balance is also below ±9% except for 3 conditions: the lowest conversion condition, the condition with T_{in} = 350 °C, and the highest flow condition with T_{in} = 450 °C when H balance is above ±10%.

The Rh is reduced in 5% H_2 in Ar at 500 °C for 1 h before testing for >4 h at the desired flow conditions. The reactor temperature is adjusted to the desired T_{in} under pure Ar flow before n-C_4H_{10} flow is introduced to the reactor followed by O_2 addition until the desired C_4H_{10}-to-O_2 equivalence ratio ϕ is reached. To avoid excessive heat release during shut-down, the O_2 flow is shut off before the C_4H_{10}. For the results presented here, the n-C_4H_{10}/O_2 ratio is consistently 0.5, which corresponds to a C/O ratio of 1.0 and a ϕ = 3.25. Experiments at a given condition are repeated at least three times with all results consistent with those shown. Results at other ϕ between 2.5 and 3.5 are reported in the earlier study [16]. Total flow rate of the gases vary from 250 to 580 sccm and for a range of T_{in} although most tests here are at T_{in} = 300 °C. Catalyst contact times τ_{res} are estimated by dividing the gas volume of the foam monolith by an average volumetric gas flow calculated using the average of T_{up} and T_{down} for the temperature and the reactor effluent mean molecular weight. The outlet composition used for calculating the volumetric flow for estimating τ_{res} was chosen because as discussed later, most of the molecular-weight-changing reactions occur very near the front face of the reactor. For cases where, T_{down} was not available, τ_{res} was not recorded. The estimated τ_{res} range from 33 to 133 ms for the 10 mm long reactor and 17–28 ms for the 5 mm long reactor as indicated in Table 1.

Reactor steady-state performance is based on n-C_4H_{10} and O_2 conversion and on product selectivities. C_4H_{10} conversion is calculated from Eq. (1):

$$\mathrm{Con}\nu_k = 1 - \frac{\dot{n}_{out} X_{k,out}}{\dot{n}_{in} X_{k,in}} = 1 - \frac{\bar{W}_{in} X_{k,out}}{\bar{W}_{out} X_{k,in}} \quad (1)$$

Table 1
Summary of CPOx reactor test conditions and performance reported in this study.

L_{reac} (mm)	Inlet (sccm)	Insu[a]	T_{in} (°C)	T_{up} (°C)	T_{down} (°C)	τ_{res} (ms)	C_4H_{10} conv.	H_2 sel.	CO sel.	$\dot{q}_{loss}$ (J/g)
10.0	250	N	300	559	453	134	0.365	0.267	0.102	1508
10.0	250	Y	300	646	528	112	0.440	0.492	0.312	1297
5.0	400	N	300	769	666	28	0.551	0.543	0.252	1236
5.0	400	Y	300	851	N/A[b]		0.782	0.907	0.830	N/A[b]
10.0	400	N	300	811[c]	522	62	0.456	0.526	0.465	1275
10.0	400	Y	300	704	574	59	0.601	0.681	0.616	1116
5.0	580	N	300	829	715	17	0.695	0.906	0.451	903
5.0	580	Y	300	910	N/A[b]		0.877	0.936	0.798	N/A[b]
10.0	580	N	300	731	550	39	0.641	0.709	0.674	1132
10.0	580	Y	300	755	608	33	0.878	0.866	0.904	651
5.0	400	N	350	850	N/A[b]		0.762	0.722	0.639	N/A[b]
10.0	400	Y	450	735	634	53	0.726	0.703	0.767	1087
10.0	580	Y	450	734	679	33	0.950	0.824	0.927	752

[a] Flag to determine if the reactor is insulated with external Al_2O_3 fiber.
[b] Thermocouple failures did not permit these measurements.
[c] Possible measurement error inconsistent with other thermocouple measurements.

where $\bar{W}_{in}$ and $\bar{W}_{out}$ are the mean molecular weights of the inlet and outlet flows and $X_{k,in}$ and $X_{k,out}$ are the inlet and outlet mole fractions determined from mass spectrometer analysis. Product selectivities $S_{k,m}$ for species k with respect to atom m is expressed by Eq. (2):

$$S_{k,m} = \frac{\nu_{k,m} X_{k,out}}{\sum_{k,out}(\nu_{k,m} X_{k,out}) - \nu_{C_4H_{10},m} X_{C_4H_{10},out} - \nu_{O_2,m} X_{O_2,out}} \quad (2)$$

where $\nu_{k,m}$ is the number of m atoms per molecule for species k. The principal selectivities used as a measure of performance in this study are those of H_2 based on H atoms ($S_{H_2,H}$ or S_{H_2}), CO based on C atoms ($S_{CO,C}$ or S_{CO}), and CO_2 based on C atoms ($S_{CO_2,C}$ or S_{CO_2}). Selectivities for carbonaceous species are based on the carbon atom unless stated otherwise.

Downstream reactor face temperature T_{down} is used to estimate the heat loss $\dot{q}_{loss}$ from the reactor by using Eq. (3) and JANAF polynomials for calculating ideal gas molar enthalpies for the inlet and outlet gas flows ($\bar{h}_{k,in}$ and $\bar{h}_{k,out}$ respectively):

$$\dot{q}_{loss} = \frac{1}{\bar{W}_{out}} \sum_{k,out} (X_{k,out} \bar{h}_{k,out}(T_{down})) - \frac{1}{\bar{W}_{in}} \sum_{k,in} (X_{k,in} \bar{h}_{k,in}(T_{in})) \quad (3)$$

$\dot{q}_{loss}$ at steady-state conditions provides an estimate for the heat lost from the flow through the outer walls of the reactor, and calculated values from Eq. (3) are provided in Table 1. The uncertainty in $\dot{q}_{loss}$ is difficult to quantify because of the sensitivity of the exhaust enthalpy due to errors in the species measurements. Nonetheless, $\dot{q}_{loss}$ provides a reasonable estimate of the amount of heat lost from the flow.

3. Results

Transient light-off of the CPOx reactor and the approach to steady-state are observed for all test conditions in this study. All cases with $\phi = 3.25$ (C/O ratio = 1.0) and $T_{in} = 300$ °C reach steady-state conditions within 10 min after introducing both fuel and O_2 into the system, and for all tests, the reactor is held at that state for 4 h or longer. Major exhaust species include CO, CO_2, H_2O, H_2, and unreacted n-C_4H_{10}. Table 1 summarizes steady-state reactor performance: T_{up} and T_{down}, C_4H_{10} conversion, S_{H_2}, and S_{CO}. Table 1 also provides estimated reactor residence times τ_{res} and heat loss per g of flow, $\dot{q}_{loss}$, calculated from Eq. (3).

All cases have steady-state O_2 conversion >98% while fuel conversion varies from 36% to 95%. Complete O_2 conversion with incomplete fuel conversion has been consistently observed for Rh-catalyzed CPOx of higher hydrocarbons [5,20,21] and indicates that C_4H_{10} dissociative adsorption must be limiting for the range of reactor temperatures in this study. Equilibrium calculations at the reactor exit temperatures (T_{down} in Table 1) suggest that over 99% of the n-C_4H_{10} should be consumed. However, competitive adsorption on the Rh surface of other species – likely O_2, CO, and/or H_2O – must prevent C_4H_{10} dissociative adsorption from reaching the equilibrium C_4H_{10} conversion in the limited reactor contact times.

Table 1 reveals significant trends in steady-state C_4H_{10} conversion, S_{H_2}, and S_{CO}. First of all, increasing total flow rate $\dot{V}_{tot,in}$ for otherwise constant reactor inlet conditions and length leads to higher fuel conversion, S_{H_2}, and S_{CO} over the range of residence times in this study. The increases with $\dot{V}_{tot,in}$ are correlated with increases in T_{down}, because increased heat loading with higher reactor flow rates is not compensated by a proportional increase in reactor heat loss. The dominant mode of heat loss is conduction through the reactor side walls, and thus heat loss will not scale with reactor flow as indicated by the decrease in $\dot{q}_{loss}$ with increasing $\dot{V}_{tot,in}$ for insulated and non-insulated reactor conditions. The associated increase in reactor temperatures with higher $\dot{V}_{tot,in}$ results in more rapid desorption and increased availability for n-C_4H_{10} adsorption and conversion.

Fig. 3a–c shows evolution of n-C_4H_{10} conversion, S_{H_2}, and S_{CO} with S_{CO_2} for the first 20 min of reaction with a constant $T_{in} = 300$ °C. After 20 min, the reactors maintain steady performance for 4 h or longer until the reactant flows are turned down. Results are shown for two reactor lengths ($L_{reac} = 5$ and 10 mm) at two flow rates ($\dot{V}_{tot,in} = 400$ and 580 sccm) for an insulated reactor configuration. In Fig. 3, a strong impact of L_{reac} on steady-state performance can be seen. Reducing L_{reac} from 10 to 5 mm results in higher steady-state C_4H_{10} conversion and S_{H_2} for the lower $\dot{V}_{tot,in}$, even as τ_{res} is reduced by more than a factor of 2. The increased conversion with reduced L_{reac} indicates that for this flow condition, C_4H_{10} adsorption and subsequent conversion occurs at the front-end of the reactor, and the rates of fuel conversion are dictated by the front-end reactor temperatures. Lower $\dot{q}_{loss}$ in the shorter reactor produces higher front-end temperatures, which increases CO desorption/oxidation and thus opens up sites for increased reaction rates and thus higher S_{H_2} as indicated in Fig. 3b. This provides more free-site availability for C_4H_{10} dissociative adsorption. This effect is less apparent at the higher $\dot{V}_{tot,in}$ due to the fact that both the shorter and longer reactors are reaching conditions where conversion and S_{H_2} are approaching their maximum values.

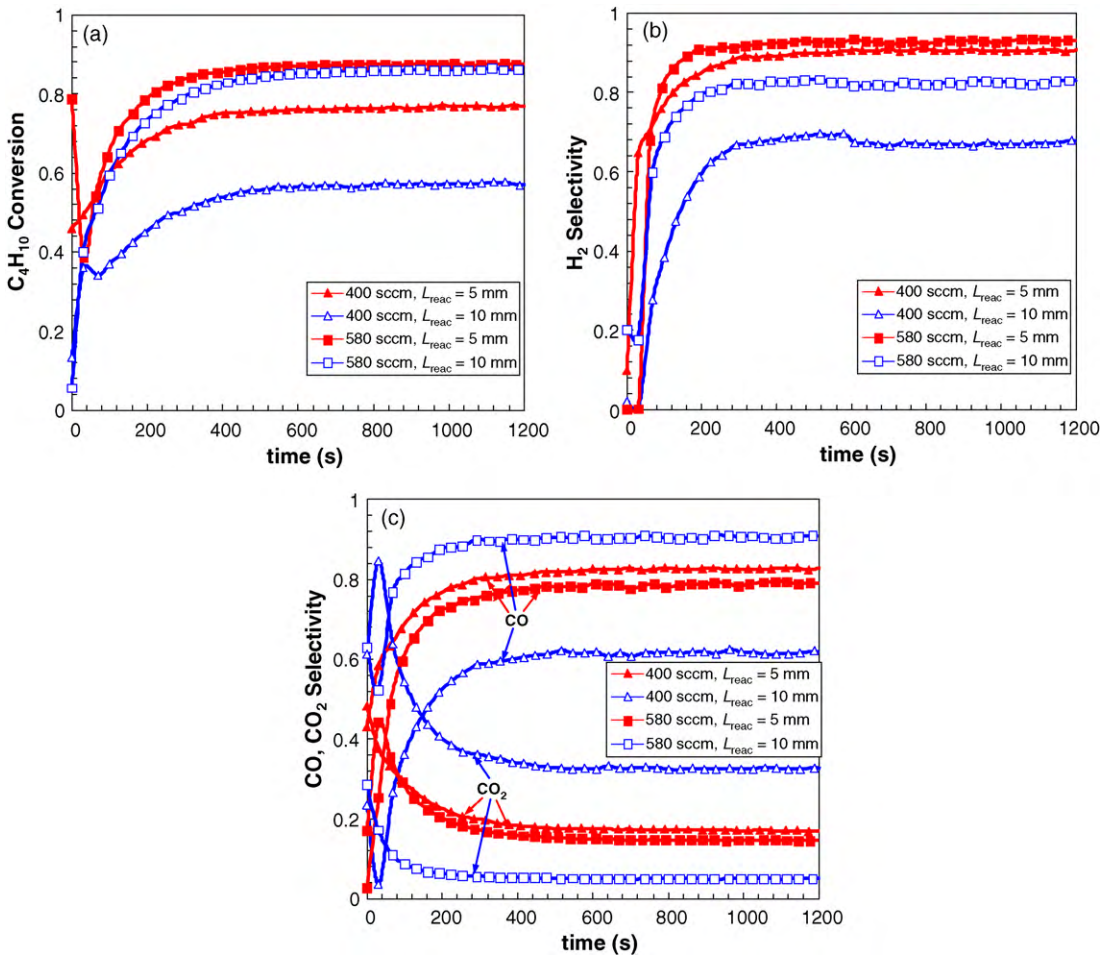

Fig. 3. Conversion and selectivities measured at insulated reactor exit for two different reactor flow rates and two reactor lengths all at fixed T_{in} = 300 °C: (a) C_4H_{10} conversion, (b) H_2 selectivity, and (c) CO and CO_2 selectivity.

Trends for S_{CO} and S_{CO_2} with $\dot{V}_{tot,in}$ and L_{reac} are illustrated in their transient evolutions in Fig. 3c. For all conditions, an initial spike in S_{CO_2} associated with the period of low fuel conversion is followed by a relatively slow decay due to increased fuel conversion and CO production. The spike in CO_2 production corresponds to the initial period of low temperature during which the Rh surface has a strong affinity for O. The high availability of O on the surface encourages complete oxidation of all adsorbed fuel species. As steady-state is approached, temperatures rise resulting in a reduction in surface O and increases in syngas (H_2 and CO) yields. For the lower $\dot{V}_{tot,in}$, higher steady-state temperatures in the shorter reactor result in higher S_{CO} and lower S_{CO_2}. However, for the higher $\dot{V}_{tot,in}$ and increased heat loading, the longer reactor produces more CO and less CO_2 than the shorter reactor. This suggests that when temperatures are high enough, additional CO is formed in the downstream region of the reactor.

The mechanism for the downstream production of CO is enlightened by looking at the mole fractions in the reactor effluent shown in Table 2. Incomplete oxidation products lumped into C^{2+} in Table 2 are produced in the front-end of the reactor as reported for other studies in the literature [22]. However, for the insulated reactor conditions in Fig. 3, effluent C^{2+} species account for less than 5% of the total C converted. Most likely, in the downstream regions of the longer reactor, endothermic reforming processes take place with H_2O and CO_2 reacting with fuel not converted in the front-end. This downstream reforming is consistent with previous observations for Rh-catalyzed C_3H_8 partial oxidation [14], but Fig. 3c suggests that downstream reforming requires adequately high reactor temperatures to drive these reactions. The higher $\dot{V}_{tot,in}$ in Fig. 3 provides adequate temperatures for downstream reforming whereas the lower $\dot{V}_{tot,in}$ does not have adequate downstream temperatures.

For the experimental tests, heat loss from the catalytic foam monolith through the Fiberfrax™ to the quartz tube walls results in steady-state T_{down} that are substantially lower than the predicted exit temperatures at adiabatic conditions. For reactor tests referred to as "insulated" in Table 1 (including those shown in Fig. 3), Al_2O_3 fiber insulation wrapped around the outside of the

Table 2
Mole fractions of insulated CPOx reactor effluent for conditions shown in Fig. 4 with T_{in} = 300 °C and ϕ = 3.25.

Product	L_{reac}			
	5.0 mm 400 sccm[a]	10.0 mm 400 sccm[a]	5.0 mm 580 sccm[a]	10.0 mm 580 sccm[a]
H_2	0.2396	0.1430	0.2694	0.2486
CH_4	0.0014	0.0017	0.0009	0.0019
n-C_4H_{10}	0.0147	0.0316	0.0081	0.0079
O_2	0.0005	0.0004	<0.0001	0.0001
CO	0.1748	0.1171	0.1832	0.2061
CO_2	0.0346	0.0622	0.0333	0.0119
H_2O	0.0224	0.0553	0.0054	0.0274
C2 + (excl. n-C_4H_{10})[b]	0.0001	0.0034	0.0045	0.0028
Ar	0.5119	0.5854	0.4953	0.4933

[a] Flow.
[b] Species detected in mass spectrometer analysis included C_2H_2, C_2H_4, C_2H_6, C_3H_6, n-C_3H_8, C_2H_4O, C_2H_5OH, CH_3CH_2CHO, $CH_3CHOHCH_3$, CH_3COCH_3.

quartz tube (but inside the furnace) minimizes reactor heat loss. However, even in those cases, there is heat conduction and radiation from the catalytic foam monolith to the tube and surroundings. For the range of insulated and non-insulated test conditions in this study, $\dot{q}_{loss}$ ranges from 650 to 1510 J/g as summarized in Table 1. These values range from 10% to 33% of the total lower heating value of the fuel. The effects of such non-adiabatic conditions have not been the focus of almost all previous CPOx studies, yet it is important to realize that many CPOx applications, such as integrated fuel processors for fuel cell technology, will inherently be impacted by non-adiabatic reactor conditions.

Transient plots of fuel conversion, S_{H_2}, and S_{CO} in Fig. 4a–c are for the same conditions as Fig. 3 but with the insulation removed. Removing the insulation for a given test condition increases $\dot{q}_{loss}$ as indicated in Table 1 for the insulated and non-insulated cases in Figs. 3 and 4 when L_{reac} = 10 mm. The increased $\dot{q}_{loss}$ occurs even though reactor temperatures decrease when the external insulation is removed as indicated by Fig. 5a and b, which plot the transient evolution of 5 and 10 mm reactor tests respectively for both insulated and non-insulated conditions. In general, removal of the insulation lowers steady-state T_{down} for the 10 mm reactor on average 70 °C.

Fig. 4a shows substantially reduced fuel conversions for the non-insulated reactor conditions in comparison to the insulated reactors in Fig. 3a. Nonetheless, the same general trends with respect to $\dot{V}_{tot,in}$ and L_{reac} are seen for the non-insulated conditions as with the insulated conditions. The reduced fuel conversion and S_{H_2} are indicative of the lower reactor temperatures for the non-insulated reactor, and Fig. 5a and b compare the transient rise to steady-state temperatures for the insulated and non-insulated reactor conditions respectively. Lower temperatures for the non-insulated cases also lead to lower S_{H_2} as shown in Fig. 4b, although the reduction is more significant for the cooler conditions at lower $\dot{V}_{tot,in}$. The lower temperatures particularly for the 400 sccm case with reduced fuel conversion and ~100% O_2 conversion provide high selectivities for H_2O and also for CO_2 as shown in Fig. 4c. Thus, increased $\dot{q}_{loss}$ inhibits C_4H_{10} adsorption and favors O_2 adsorption, thereby providing an increased affinity for complete oxidation products. As $\dot{q}_{loss}$ is decreased and reactor temperature rises, S_{H_2} rises substantially first, before S_{CO}, as exemplified by the case at 580 sccm with L_{reac} = 5 mm. For that case, steady state S_{H_2} is above 90% while S_{CO} remains below 50%. The stronger binding energies of CO on Rh [23] encourage CO oxidation over H oxidation when surface O is still available due to incomplete C_4H_{10} adsorption.

Significant differences in performance between the L_{reac} = 5 and 10 mm have been largely explained by changes in reactor temperatures. These changes are highlighted in Fig. 5a and b which shows T_{up} and T_{down} for the 5 and 10 mm reactors respectively. The values for T_{down} of the 5 mm reactor under the hottest insulated conditions are not shown due to thermocouple failures during reactor testing. All the same, comparing the two figures shows the consistently higher T_{up} and T_{down} for the 5 mm reactor due to its reduced heat loss through the side walls. Not only are the steady-state temperatures higher, but the rates of reactor temperature rise are also much higher for the shorter reactor, which is beneficial for integration with SOFC applications where start-up time and efficiencies are critical.

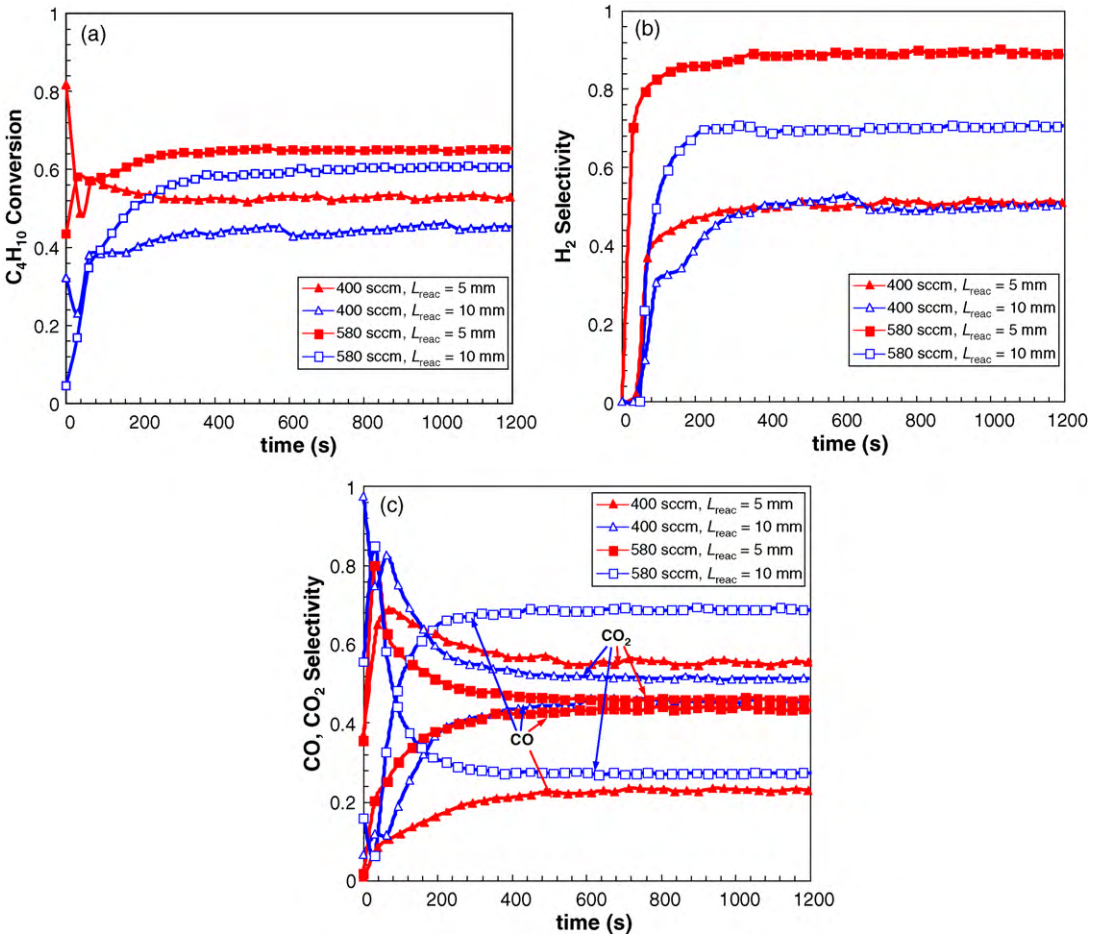

Fig. 4. Conversion and selectivities measured at non-insulated reactor exit for two different reactor flow rates and two reactor lengths all at fixed T_{in} = 300 °C: (a) C_4H_{10} conversion, (b) H_2 selectivity, and (c) CO and CO_2 selectivity.

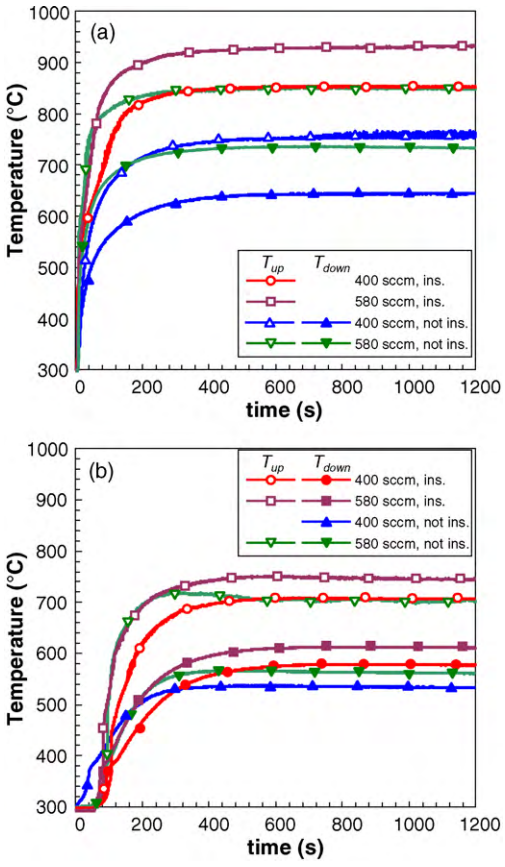

Fig. 5. Transient evolution of T_{up} and T_{down} face temperatures for an insulated reactor performance at a fixed $\phi = 3.25$ and $T_{in} = 300\ ^{\circ}C$: (a) $L_{reac} = 5$ mm and (b) $L_{reac} = 10$ mm. Some temperatures are not shown due to failed thermocouple readings.

Fig. 5 also shows how increases in $\dot{V}_{tot,in}$ result in higher temperatures and more rapid start-up for T_{up}. For these cases, the trend of continued increase in fuel conversion and syngas selectivities with $\dot{V}_{tot,in}$ suggest that τ_{res} can go smaller before the trend with conversion and $\dot{V}_{tot,in}$ will be reversed. Fig. 6 plots C_4H_{10} conversion, S_{H_2}, and S_{CO} vs. reactor flow rate for all $T_{in} = 300\ ^{\circ}C$ cases presented in this study. Increasing $\dot{V}_{tot,in}$ over the range in Fig. 6 for the non-insulated cases always provides higher conversion due to reduced $\dot{q}_{loss}$ and higher temperatures. Predicting the point at which τ_{res} becomes too short to sustain adequate reactivity is beyond the scope of this study due to the fact that a full temperature profiles are needed to implement global rate expressions or detailed reaction mechanisms to predict conversion and selectivities. Currently, no such kinetic models are provided in the literature. Certainly smaller τ_{res} have been employed in other studies on propane CPOx on Rh in the literature for near adiabatic conditions [24]. However, it will be beneficial to provide reactor designers a plot of how performance varies with τ_{res} as a function of reactor heat loss per unit flow since many applications will not be adiabatic.

For the highest $\dot{V}_{tot,in} = 580$ sccm, the insulated reactor performance at $T_{in} = 300\ ^{\circ}C$ reaches fuel conversion of 88% for both L_{reac}. S_{H_2} is higher for the shorter reactor 94–87%, but S_{CO} is less 80–90%. Such high fuel conversion is comparable to that from similar conditions tested with C_3H_8 as the fuel [5], but the current studies showed higher S_{H_2} and S_{CO} and reduced hydrocarbon byproducts. This is likely because the tests for C_3H_8 CPOx were done with higher T_{in} (up to 700 °C) and thus incurred more gas-phase reactions, which tend to be much less selective toward syngas products [25]. It should be noted that for the shorter reactor

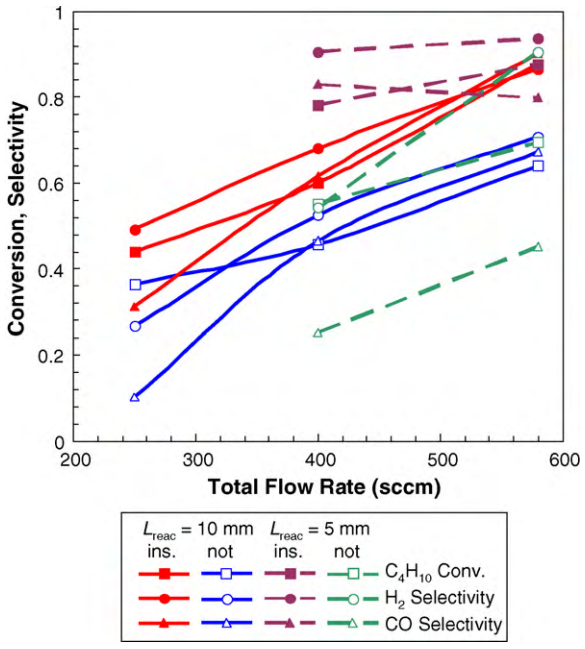

Fig. 6. Steady-state reactor performance including C_4H_{10} conversion, H_2 selectivity, and CO selectivity vs. reactor flow rate at a fixed $\phi = 3.25$ and $T_{in} = 300\ ^{\circ}C$ for $L_{reac} = 5$ and 10 mm.

in this study, the C^{2+} hydrocarbons increased when heat loss from the reactor is increased by removing the insulation. Table 3 shows the effluent species fractions for the non-insulated reactor cases plotted in Fig. 4. For the 400 and 580 sccm cases with $L_{reac} = 5$ mm, approximately 20% and 10% respectively of the converted fuel carbon is found in the C^{2+} species which are a mixture of oxygenates and unsaturated hydrocarbons. It is possible that these species form from gas-phase reactions and are not adequately consumed in the downstream part of the reactor when $\dot{q}_{loss}$ increases. Further studies are necessary to explore this. However, increased L_{reac} tends to destroy any such species as indicated by the low C^{2+} species fractions for the $L_{reac} = 10$ mm cases in Table 3.

The reactor temperatures and residence times in this study do not result in significant CH_4 production ($S_{CH_4} < 0.5\%$) for all cases with $T_{in} = 300\ ^{\circ}C$. To test the effects of T_{in} on CH_4 production and other reactor performance metrics, tests are conducted with T_{in} up to 450 °C. The higher T_{in} (450 °C) does produce more CH_4 with S_{CH_4} around 1.0% but these values are still much smaller than for the comparable C_3H_8 tests with $T_{in} = 700\ ^{\circ}C$ as reported in the literature [5]. This is evidence for limited gas-phase reactions which are known to produce significant CH_4 under rich conditions

Table 3
Mole fractions of non-insulated CPOx reactor effluent for conditions shown in Fig. 4 with $T_{in} = 300\ ^{\circ}C$ and $\phi = 3.25$.

Product	L_{reac}			
	5.0 mm 400 sccm[a]	10.0 mm 400 sccm[a]	5.0 mm 580 sccm[a]	10.0 mm 580 sccm[a]
H_2	0.1215	0.0772	0.2272	0.1574
CH_4	0.0010	<0.0001	0.0006	0.0017
n-C_4H_{10}	0.0364	0.0493	0.0220	0.0272
O_2	0.0012	0.0001	<0.0001	0.0002
CO	0.0449	0.0769	0.0906	0.1309
CO_2	0.0972	0.0847	0.0912	0.0555
H_2O	0.0666	0.0661	0.0059	0.0562
C^{2+} (excl. n-C_4H_{10})[b]	0.0127	0.0027	0.0069	0.0022
Ar	0.6185	0.6432	0.5556	0.5689

[a] Flow.
[b] Species detected in mass spectrometer analysis included C_2H_2, C_2H_4, C_2H_6, C_3H_6, n-C_3H_8, C_2H_4O, C_2H_5OH, CH_3CH_2CHO, $CH_3CHOHCH_3$, CH_3COCH_3.

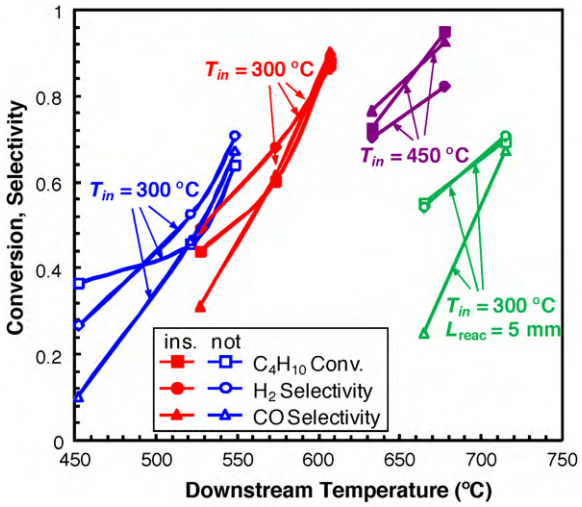

Fig. 7. Measured C_4H_{10} conversion and selectivities of both H_2 and CO vs. measured temperature at the exit face of catalytic reactor for fixed ϕ = 3.25. All cases are for L_{reac} = 10 mm unless indicated otherwise. Open symbols are for non-insulated reactors and closed symbols are for insulated reactors.

[25]. Gas-phase reactivity tests with washcoated supports without Rh impregnation confirmed this as reported in the earlier study [16].

Increase of T_{in} from 300 to 450 °C for the 10 mm does increase the reactor temperatures as shown in Table 1 and plotted in Fig. 7. The increased T_{in} provides higher fuel conversion and higher S_{CO} at both 400 and 580 sccm flow rates but it does not lead to higher S_{H_2}. The increase in T_{in} results in higher T_{down} (by ≈70 °C) than for T_{in} = 300 °C at the same flow rates. Earlier studies with C_3H_8 partial oxidation over supported Rh catalysts observed a stronger increase in S_{CO} than S_{H_2} with reactor inlet temperature [5,26]. The higher sensitivity of S_{CO} with inlet temperature conditions in comparison to S_{H_2} suggests that the competition between CO desorption and CO oxidation is strongly temperature dependent and further confirms that CO desorption has a higher E_{act} than H_2 desorption.

4. Discussion

Previous Rh-based CPOx studies have concluded that upstream complete fuel oxidation (surface-catalyzed and/or gas-phase) in the first mm or so of the reactor is followed by subsequent downstream endothermic reforming. However, it may be helpful to consider trends observed in this study in terms of adsorption and desorption of principal reactants and products. Fuel conversion is likely controlled by fuel adsorption limitations due to lack of available sites. Increasing upstream reactor temperature, either via higher T_{in} or otherwise, results in faster removal of surface O and CO atoms [23] due to oxidation and desorption. This allows for higher fuel adsorption and dissociation as well as further production of H_2 and CO.

Fig. 7 shows the correlation between reactor exit temperature T_{down} and fuel conversion, S_{H_2}, and S_{CO} all for cases in this study (with C/O atomic ratios = 1.0). The plot includes cases for both non-insulated reactors and insulated reactors at both L_{reac} and T_{in}. Generally, higher T_{down} are accompanied by increased fuel conversion, S_{H_2}, and S_{CO}.

Modeling of CH_4 CPOx reactors with Rh catalyst has shown that increased flow rates increase the width of the high-temperature region (for the solid) in the upstream portion of the reactor [6]. This increased length of high-temperature increases fuel conversion and desorption of partial oxidation products leading to the trends illustrated in Fig. 7. These trends in reactor temperatures with flow rates are accentuated when heat loss occurs at the reactor boundaries. In catalytic foam reactors, the dominant heat loss mechanisms are conduction and radiation, neither of which depends directly on flow rate. As long as the contact times are adequately long to maintain full O_2 conversion and high fuel conversion, higher flow rates will provide higher temperatures due to lower $\dot{q}_{loss}$. This results in more effective removal of surface O and shifts the product distribution to higher H_2 and CO yields.

Fig. 7 also indicates that factors other than just reactor temperatures must influence both fuel conversion and product selectivity. For example, the higher T_{in} = 450 °C cases produce the highest T_{down} but at the lower 400 sccm flow rate, fuel conversion, S_{H_2} and S_{CO} are significantly lower than for the case with T_{in} = 300 °C, flow rate at 580 sccm, and a significantly lower T_{down}. The lower fuel conversion rates at the higher T_{in} = 450 °C and lower flow rate implies that heat release in the reactor front-end is more important for achieving high conversion than inlet temperature. This suggests the importance of developing higher hydrocarbon surface dissociation models to explore these trends for reactor design.

Another interesting result in Fig. 7 is the deviation from the general trends for the non-insulated case with the shorter L_{reac} = 5 mm. Although these cases have the highest downstream temperatures, they have lower fuel conversion, S_{H_2} and S_{CO}. This confirms that the downstream portion of the reactor plays a role in driving reactions particularly related to CO production. When the reactor is not adequately long or hot to drive fuel conversions very high in the front-end reaction zone, the O_2 is completely converted with relatively high selectivity toward CO_2 even with substantial H_2 yield. This is further verified by noting how as fuel conversion drops to near 50% or lower for cases in Fig. 7, S_{CO} drops off much more rapidly. It should be noted, that for the insulated L_{reac} = 5 mm the reactor becomes adequately hot in the front-end to compress the fuel conversion zone with high conversion, S_{H_2}, and S_{CO}.

Considering the integration of CPOx reactors with SOFCs, Fig. 7 indicates that conditions of relatively high heat loss and low fuel conversion result in significant CO_2 concentrations out of the CPOx reactor. For higher hydrocarbons, this can be problematic for a downstream SOFC anode. Limited availability of H_2O at the anode inlet implies the need for "dry" CO_2 reforming to prevent fuel pyrolysis and carbon deposition in the SOFC anode. Rates for dry reforming are known to be relatively slow on typical SOFC anode materials (Ni-YSZ) [27]. As such, CPOx reactor design must ensure high fuel conversion for integration with SOFC's, or SOFC anodes with higher resistance to carbon deposition must be developed as proposed by some [1,28].

The importance of heat loss on reactor performance is highlighted in Fig. 8, which plots fuel conversion and S_{H_2} as a function of heat loss per unit mass of flow $\dot{q}_{loss}$. The impact of reactor heat loss on fuel conversion and product selectivity provides some key insights for CPOx research and development efforts. First of all, it is important that kinetic studies be coupled with measured axial reactor temperature profiles as done recently for CH_4 CPOx on Rh-based catalysts [6,17]. These studies are needed to develop higher hydrocarbon dissociative adsorption mechanisms that can be coupled to previous microkinetic models for CH_4 CPOx [6,15,23,29]. Secondly, this study indicates that a traditional view of CPOx reactors in terms of direct and indirect partial oxidation may not adequately capture the performance of such reactors particularly at conditions of high heat loss and lower fuel conversion where the full conversion of O_2 can lead to high H_2 and CO_2 production. It may be rather beneficial to consider the competition between adsorption and desorption of major reactants and products to develop a general kinetic understanding that captures the behavior of Rh-based CPOx reactors at conditions expected in non-adiabatic systems. Such conditions will certainly exist in many small-scale applications such as SOFC systems, and

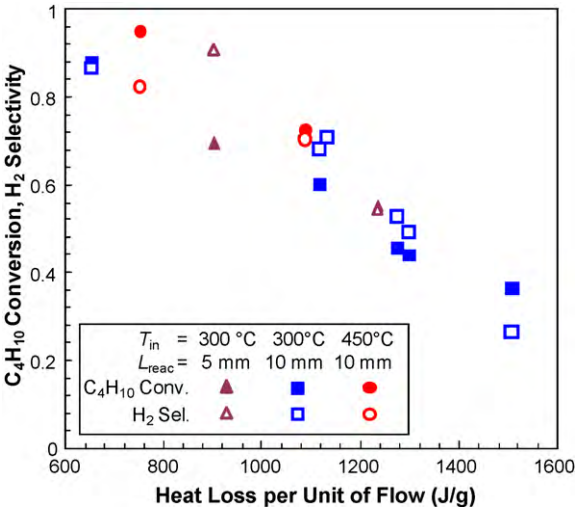

Fig. 8. Conversion of C_4H_{10} and H_2 selectivity vs. calculated heat loss rate per unit flow (in J/g) for a fixed $\phi = 3.25$ and different inlet temperatures. Data include a range of flow rates and both insulated and non-insulated reactors.

as such, it is important to develop the needed microkinetic models for improved reactor and overall system design.

5. Conclusion

Studies of n-C_4H_{10} CPOx over Rh/Al_2O_3-supported catalyst (all at a C/O atomic ratio = 1.0) have indicated that non-adiabatic reactor conditions can play a significant role in fuel conversion and product distributions. Many of the trends observed in this study can be related to the correlation between downstream reactor temperature and performance with fuel conversion and syngas selectivities generally rising with reactor temperature. In addition, increased flow rates (even with their lower τ_{res}) tend to further enhance performance with reduced heat loss per unit mass of flow. This effect seems to be due to higher rates of fuel conversion and thus removal of surface O for increased reaction rates. In addition, reactor length plays a counterintuitive role in this system. For the range of τ_{res} studied here, the shorter reactor (5 mm vs. 10 mm) produced, for the same conditions, higher conversions and H_2 selectivity in comparison to the longer reactor. This effect was due to reduced heat loss out the sides of the reactor and thus higher reactor temperatures. The results however did show that at conditions of lower fuel conversion (~50% or lower), the shorter reactor produced lower CO selectivity which implies that downstream conversion of CO_2 to CO is likely occurring at such conditions although the mechanism remains unclear.

These studies indicate the need to develop adequate higher hydrocarbon CPOx mechanisms for reactor design. However, these mechanisms must be validated by experimental studies which properly account for heat loss in reactors by carefully measuring axial temperature profiles through the length of the CPOx reactor. The results of this study suggest that the global views of direct and indirect CPOx may not be the most effective way of predicting reactor performance particularly at high heat loss conditions with relatively low fuel conversion. Under such conditions high selectivities to H_2 and CO_2 indicate that neither a direct nor indirect route accurately captures the product distribution. Rather reaction rates seem to be governed by the competition between adsorption and desorption of major reactants and products. Developing a microkinetic model will be invaluable for fully understanding how CPOx reactors will perform in non-adiabatic applications. This will be vital for building optimized fuel processing systems for many applications such as small-scale SOFC's that will provide adequate performance in both transient and steady-state operating conditions.

Acknowledgement

The financial support from Minta Martin Foundation at the University of Maryland is gratefully acknowledged.

References

[1] S. McIntosh, R.J. Gorte, Chem. Rev. 104 (2004) 4845.
[2] B.D. Madsen, S.A. Barnett, Solid State Ionics 176 (2005) 2545.
[3] A. Weber, B. Sauer, A.C. Muller, D. Herbstritt, E. Ivers-Tiffee, Solid State Ionics 152 (2002) 543.
[4] R.J. Kee, H.Y. Zhu, A.M. Sukeshini, G.S. Jackson, Combust. Sci. Technol. 180 (2008) 1207.
[5] I. Aartun, B. Silberova, H. Venvik, P. Pfeifer, O. Gorke, K. Schubert, A. Holmen, Catal. Today 105 (2005) 469.
[6] I. Tavazzi, A. Beretta, G. Groppi, P. Forzatti, J. Catal. 241 (2006) 1.
[7] I. Tavazzi, M. Maestri, A. Beretta, G. Groppi, E. Tronconi, P. Forzatti, AIChE J. 52 (2006) 3234.
[8] R.P. O'Connor, E.J. Klein, D. Henning, L.D. Schmidt, Appl. Catal. A: Gen. 238 (2003) 29.
[9] R.P. O'Connor, E.J. Klein, L.D. Schmidt, Catal. Lett. 70 (2000) 99.
[10] M. Huff, P.M. Torniainen, L.D. Schmidt, Catal. Today 21 (1994) 113.
[11] A.G. Dietz, A.F. Carlsson, L.D. Schmidt, J. Catal. 176 (1998) 459.
[12] A. Bodke, D. Henning, L.D. Schmidt, Catal. Today 61 (2000) 65.
[13] N. Hotz, M.J. Stutz, S. Loher, W.J. Stark, D. Poulikakos, Appl. Catal. B: Environ. 73 (2007) 336.
[14] B. Silberova, H.J. Venvik, A. Holmen, Catal. Today 99 (2005) 69.
[15] C. Appel, J. Mantzaras, R. Schaeren, R. Bombach, A. Inauen, N. Tylli, M. Wolf, T. Griffin, D. Winkler, R. Carroni, Proc. Combust. Inst. 30 (2005) 2509.
[16] S.A. Seyed-Reihani, G.S. Jackson, Appl. Catal. A: Gen. 353 (2008) 181.
[17] A. Schneider, J. Mantzaras, S. Eriksson, Combust. Sci. Technol. 180 (2008) 89.
[18] O. Deutschmann, L.D. Schmidt, AIChE J. 44 (1998) 2465.
[19] M. Bizzi, G. Saracco, R. Schwiedernoch, O. Deutschmann, AIChE J. 50 (2004) 1289.
[20] A.S. Bodke, S.S. Bharadwaj, L.D. Schmidt, J. Catal. 179 (1998) 138.
[21] R. Subramanian, G.J. Panuccio, J.J. Krummenacher, I.C. Lee, L.D. Schmidt, Chem. Eng. Sci. 59 (2004) 5501.
[22] D.I. Iordanoglou, A.S. Bodke, L.D. Schmidt, J. Catal. 187 (1999) 400.
[23] R. Schwiedernoch, S. Tischer, C. Correa, O. Deutschmann, Chem. Eng. Sci. 58 (2003) 633.
[24] L.D. Schmidt, E.J. Klein, C.A. Leclerc, J.J. Krummenacher, K.N. West, Chem. Eng. Sci. 58 (2003) 1037.
[25] G.K. Gupta, A.M. Dean, K. Ahn, R.J. Gorte, J. Power Sources 158 (2006) 497.
[26] A. Beretta, P. Forzatti, Chem. Eng. J. 99 (2004) 219.
[27] H.Y. Zhu, R.J. Kee, V.M. Janardhanan, O. Deutschmann, D.G. Goodwin, J. Electrochem. Soc. 152 (2005) A2427.
[28] E.P. Murray, S.J. Harris, J. Liu, S.A. Barnett, Electrochem. Solid State Lett. 9 (2006) A292.
[29] S.R. Deshmukh, D.G. Vlachos, Combust. Flame 149 (2007) 366.